J|A|C|S
ARTICLES
Published on Web 04/24/2002

Electron-Transfer Mechanisms through Biological Redox Chains in Multicenter Enzymes

Lars J. C. Jeuken,[†] Anne K. Jones,[†] Stephen K. Chapman,[‡] Gary Cecchini,[§] and Fraser A. Armstrong*[,†]

Contribution from the Inorganic Chemistry Laboratory, Oxford University, South Parks Road, OX1 3QR, Oxford, United Kingdom, Department of Chemistry, University of Edinburgh, West Mains Road, Edinburgh EH9 3JJ, Scotland, United Kingdom, and Molecular Biology Division, DVA Medical Center and Department of Biochemistry and Biophysics, University of California, San Francisco, California 94121

Received December 3, 2001

Abstract: A new approach for studying intramolecular electron transfer in multicenter enzymes is described. Two fumarate reductases, adsorbed on an electrode in a fully active state, have been studied using square-wave voltammetry as a kinetic method to probe the mechanism of the long-range electron transfer to and from the buried active site. Flavocytochrome c_3 (Fcc_3), the globular fumarate reductase from *Shewanella frigidimarina*, and the soluble subcomplex of the membrane-bound fumarate reductase of *Escherichia coli* (FrdAB) each contain an active site FAD that is redox-connected to the surface by a chain of hemes or Fe−S clusters, respectively. Using square-wave voltammetry with large amplitudes, we have measured the electron-transfer kinetics of the FAD cofactor as a function of overpotential. The results were modeled in terms of the FAD group receiving or donating electrons either via a direct mechanism or one involving hopping via the redox chain. The FrdAB kinetics could be described by both models, while the Fcc_3 data could only be fit on the basis of a direct electron-transfer mechanism. This raises the likelihood that electron transfer can occur via a superexchange mechanism utilizing the heme groups to enhance electronic coupling. Finally, the FrdAB data show, in contrast to Fcc_3, that the maximum ET rate at high overpotential is related to the turnover number for FrdAB measured previously so that electron transfer is the limiting step during catalysis.

Introduction

In contrast to atoms and molecules, electrons can tunnel across long distances (∼14 Å) without this being rate-limiting in most biological systems.[1] However, there are many examples of enzymes in which electron transfer (ET) over even longer ranges (>15 Å) is necessary. This problem is resolved by the use and positioning of redox centers such as hemes (Fe−porphyrins) or iron−sulfur clusters between the initial donor and final acceptor sites (i.e., a donor−bridge−acceptor system). The resulting configuration is referred to as a biological "wire" or redox chain. Although these redox chains are commonplace in enzymes (for instance, hydrogenases,[2,3] CO dehydrogenase,[4] photosynthetic reaction centers,[5,6] and cytochrome *c* oxidases;[7,8] see also ref 1 and references therein), the mechanism by which they mediate electron transfer remains unestablished in most cases.

Studies of long-range electron transfer (>15 Å) have recently received interest through related work on DNA.[9−15] Theoretical research has led to two proposed mechanisms for ET along DNA nucleotides (see Figure 1).[16−20] First, electrons may be trans-

* To whom correspondence should be addressed. E-mail: Fraser.Armstrong@chem.ox.ac.uk. Fax: 0044-(0)1865-272690.
[†] Oxford University.
[‡] University of Edinburgh.
[§] University of California.

(1) Page, C. C.; Moser, C. C.; Chen, X. X.; Dutton, P. L. *Nature* **1999**, *402*, 47−52.
(2) Volbeda, A.; Charon, M. H.; Piras, C.; Hatchikian, E. C.; Frey, M.; Fontecillacamps, J. C. *Nature* **1995**, *373*, 580−587.
(3) Peters, J. W.; Lanzilotta, W. N.; Lemon, B. J.; Seefeldt, L. C. *Science* **1998**, *282*, 1853−1858.
(4) Dobbek, H.; Svetlitchnyi, V.; Gremer, L.; Huber, R.; Meyer, O. *Science* **2001**, *293*, 1281−1285.
(5) Ermler, U.; Fritzsch, G.; Buchanan, S. K.; Michel, H. *Structure* **1994**, *2*, 925−936.
(6) Schubert, W. D.; Klukas, O.; Krauss, N.; Saenger, W.; Fromme, P.; Witt, H. T. *J. Mol. Biol.* **1997**, *272*, 741−769.
(7) Tsukihara, T.; Aoyama, H.; Yamashita, E.; Tomizaki, T.; Yamaguchi, H.; Shinzawaitoh, K.; Nakashima, R.; Yaono, R.; Yoshikawa, S. *Science* **1995**, *269*, 1069−1074.
(8) Iwata, S.; Ostermeier, C.; Ludwig, B.; Michel, H. *Nature* **1995**, *376*, 660−669.
(9) Kelley, S. O.; Barton, J. K. *Science* **1999**, *283*, 375−381.
(10) Dandliker, P. J.; Holmlin, R. E.; Barton, J. K. *Science* **1997**, *275*, 1465−1468.
(11) Hall, D. B.; Holmlin, R. E.; Barton, J. K. *Nature* **1996**, *382*, 731−735.
(12) Lewis, F. D.; Letsinger, R. L.; Wasielewski, M. R. *Acc. Chem. Res.* **2001**, *34*, 159−170.
(13) Wagenknecht, H. A.; Stemp, E. D. A.; Barton, J. K. *Biochemistry* **2000**, *39*, 5483−5491.
(14) Arkin, M. R.; Stemp, E. D. A.; Holmlin, R. E.; Barton, J. K.; Hormann, A.; Olson, E. J. C.; Barbara, P. F. *Science* **1996**, *273*, 475−480.
(15) Giese, B.; Amaudrut, J.; Köhler, A.-K.; Spormann, M.; Wessely, S. *Nature* **2001**, *412*, 318−320.
(16) Grozema, F. C.; Berlin, Y. A.; Siebbeles, L. D. A. *J. Am. Chem. Soc.* **2000**, *122*, 10903−10909.
(17) Voityuk, A. A.; Rosch, N.; Bixon, M.; Jortner, J. *J. Phys. Chem. B* **2000**, *104*, 9740−9745.
(18) Bixon, M.; Giese, B.; Wessely, S.; Langenbacher, T.; Michel-Beyerle, M. E.; Jortner, J. *Proc. Natl. Acad. Sci. U.S.A.* **1999**, *96*, 11713−11716.
(19) Zusman, L. D.; Beratan, D. N. *J. Chem. Phys.* **1999**, *110*, 10468−10481.

10.1021/ja012638w CCC: $22.00

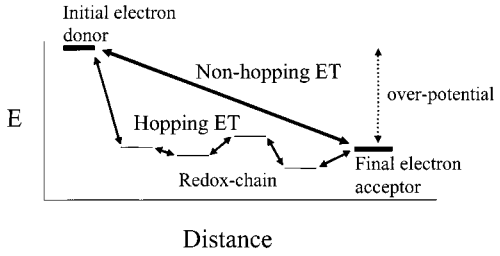

Figure 1. Representations of electron transfer via a nonhopping and a hopping mechanism in a donor−bridge (i.e., redox chain)−acceptor system.

ferred from the donor group onto the DNA, after which they hop from nucleotide to nucleotide (changing the *formal* oxidation state of each nucleotide) until they are transferred to the acceptor group, that is, a hopping mechanism. Alternatively, electrons may tunnel *directly* from donor to acceptor via a superexchange mechanism that is sensitive to the overlap and energies of the frontier orbitals in the chain.

For multicenter enzymes, it is tacitly assumed that intramolecular electron transfer occurs via a hopping mechanism. In principle, this assumption can be tested by measuring the ET rate as a function of driving force between the donor and final acceptor. Using an electrode, this driving force can be varied continuously. Two limiting cases can be defined: if the electrons transfer directly, the rate should increase with driving force (equal to the potential difference between donor and acceptor) in accordance with the Butler−Volmer and Marcus theories. For clarity, we will refer to this as the "nonhopping" mechanism. In contrast, if electrons are transferred via a hopping mechanism, the rate of electron transfer will ultimately be controlled by the rate *constant* for ET between the redox-chain component and the acceptor, which is *independent* of the electrode potential.

To gain further insight into the mechanism of ET along biological redox chains, we have studied the electrochemical kinetics of two multicenter enzymes. The first of these is the globular fumarate reductase from *Shewanella frigidimarina*, called flavocytochrome c_3 (Fcc_3), which is a 64 kDa protein with four hemes in the redox chain and a noncovalently bound flavin group (FAD) in the active site (see Figure 2).[21] The second enzyme is the fumarate reductase from *Escherichia coli*, which in its membrane-bound form is a tetramer (FrdABCD), containing one or two quinone binding sites (electron donor), three Fe−S clusters in the redox chain, and a covalently attached FAD in the active site (see Figure 2).[22] Here, we have used the soluble subcomplex (93 kDa) of fumarate reductase (FrdAB) that lacks the membrane anchors and the quinone binding sites (FrdC and FrdD) but contains all the Fe−S clusters (FrdB) as well as the FAD group (FrdA). In both enzymes, the active site FAD is buried within the protein (>15 Å from the surface when measured with a 10 Å diameter probe, see later), whereas several of the hemes (Fcc_3) or one of the Fe−S clusters (FrdAB) of the respective redox chains are exposed to the surface. The assumption, therefore, is that these redox chains somehow facilitate electron transfer to the FAD.

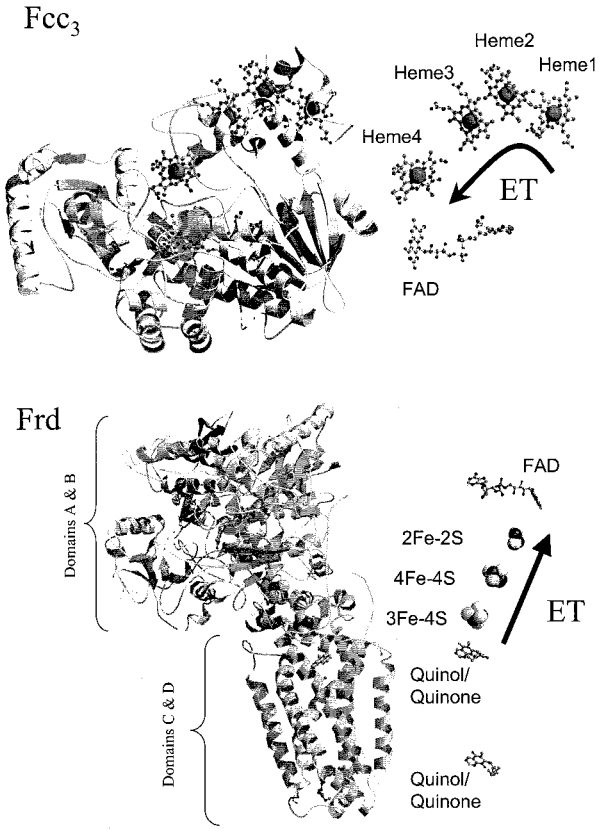

Figure 2. (Top) Representation[63,64] of fumarate reductase from *S. frigidimarina* (Fcc_3),[21] showing the full structure and (at right) the redox active groups. (Bottom) Representation[63,64] of fumarate reductase from *E. coli*[22] showing the full and (at right) the redox active groups.

Fcc_3 and FrdAB adsorbed on pyrolytic graphite edge (PGE) electrodes give well-defined cyclic voltammetry (CV) signals and are fully active in the presence of substrate.[23−28] Studying enzymes electrochemically while adsorbed at an electrode (protein film voltammetry) is a unique way of extracting information on their ET and catalytic properties.[29] For both these enzymes, the active site FAD can be distinguished clearly from the components of the redox chain since it exhibits a cooperative two-electron transfer reaction (the semiquinone radical state is relatively unstable) that at low scan rates yields a much sharper signal.[30]

Previously, we have shown that square-wave voltammetry (SWV, see Figure 3) utilizing large amplitudes (75−300 mV)

(20) Jortner, J.; Bixon, M.; Langenbacher, T.; Michel-Beyerle, M. E. *Proc. Natl. Acad. Sci. U.S.A.* **1998**, *95*, 12759−12765.
(21) Taylor, P.; Pealing, S. L.; Reid, G. A.; Chapman, S. K.; Walkinshaw, M. D. *Nat. Struct. Biol.* **1999**, *6*, 1108−1112.
(22) Iverson, T. M.; Luna-Chavez, C.; Cecchini, G.; Rees, D. C. *Science* **1999**, *284*, 1961−1966.
(23) Turner, K. L.; Doherty, M. K.; Heering, H. A.; Armstrong, F. A.; Reid, G. A.; Chapman, S. K. *Biochemistry* **1999**, *38*, 3302−3309.
(24) Jones, A. K.; Camba, R. O.; Reid, G. A.; Chapman, S. K.; Armstrong, F. A. *J. Am. Chem. Soc.* **2000**, *122*, 6494−6495.
(25) Heering, H. A.; Weiner, J. H.; Armstrong, F. A. *J. Am. Chem. Soc.* **1997**, *119*, 11628−11638.
(26) Sucheta, A.; Cammack, R.; Weiner, J.; Armstrong, F. A. *Biochemistry* **1993**, *32*, 5455−5465.
(27) Léger, C.; Heffron, K.; Pershad, H. R.; Maklashina, E.; Luna-Chavez, C.; Cecchini, G.; Ackrell, B. A. C.; Armstrong, F. A. *Biochemistry* **2001**, *40*, 11234−11245.
(28) Armstrong, F. A.; Camba, R.; Heering, H. A.; Hirst, J.; Jeuken, L. J. C.; Jones, A. K.; Léger, C.; McEvoy, J. P. *Faraday Discuss.* **2000**, *116*, 191−203.
(29) Armstrong, F. A.; Heering, H. A.; Hirst, J. *Chem. Soc. Rev.* **1997**, *26*, 169−179.
(30) The peak shape is dependent on the apparent n value, n_{app}, which reflects the extent of cooperativity of electron transfer. The half-height peak width can be calculated by $\delta = 3.53 \times (RT/n_{app}F)$. The maximum current is given by $i_p = n_s n_{app} F^2 \nu A\Gamma/RT$, with n_s the stoichiometric number of electrons, A the electrode area, and Γ the electroactive protein coverage.[29] Thus, for $n_{app} = 2$, peaks are twice as sharp and four times as high as peaks with $n = 1$.

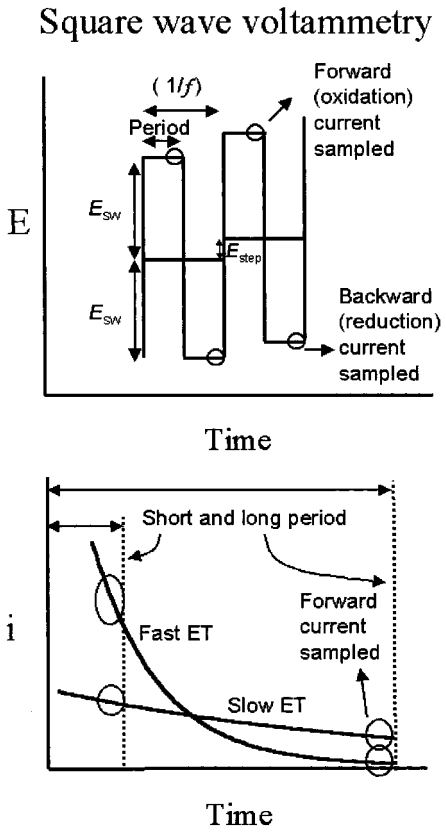

Figure 3. (Top) Variation of potential with time for a square-wave voltammetry experiment. (Bottom) Two examples of current traces within a period of a square-wave voltammetry experiment. For each example, the sampling points for two different frequencies (i.e., periods) of a square-wave voltammogram are indicated by circles.

is a good method for measuring ET kinetics as a function of driving force.[31] The important benefit of SWV is that it combines the kinetic information obtained by chrono-amperometry with the ease and accuracy of background subtraction common for linear-sweep voltammetry. Here, we have used SWV to probe the mechanism of ET to the buried FAD groups in the two fumarate reductases, noting that significant differences are expected for the two ET mechanisms outlined above. First, we will show how the SWV response is expected to vary depending on whether a hopping or nonhopping mechanism is operating. We will then describe and discuss the results that are obtained for the two fumarate reductases.

Materials and Methods

Proteins and Solutions. Recombinant fumarate reductase[32] from *Shewanella frigidimarina* NCIMB400 (Fcc_3) was expressed in *S. frigidimarina* strain EG301 and purified as described previously.[33] The recombinant soluble domain of *E. coli* fumarate reductase (FrdAB) was modified with a His-tag to facilitate purification.[27] Deionized water (Millipore, 18 M Ω cm) was used throughout the voltammetric experiments, and all chemicals were purchased from either Sigma or Merck (BDH, AnalaR). For all experiments, a mixed buffer system was used (25 mM MES, HEPES, PIPES, and TAPS) with 0.1 M NaCl as supporting electrolyte. Measurements were made at 10 °C, at which temperature the pH values of cell solutions were measured and adjusted and then checked after the experiment. Polymyxin B sulfate (200 μg/mL) was included as a coadsorbate to stabilize the protein layer on the PGE electrode. In contrast to CV experiments, the SWV pulse sequence with large switching amplitudes destabilized the FrdAB film, but this problem could be minimized by adding 20% glycerol (volume/total volume). Fast scan CV experiments showed that the addition of glycerol did not change the ET kinetics, although it slightly decreased electrode coverage. Fcc_3 films were sufficiently stable to perform SWV experiments without the addition of glycerol.

Electrodes. PGE and rotating disk PGE working electrodes were constructed as described previously.[26,34] The disk of pyrolytic graphite (Advanced Ceramics Corp., Wales) was housed in a Teflon sheath so that the edge plane is oriented to contact the solution (i.e., the basal -*ab* plane is normal to the solution surface). Typically, the electrode area was minimized to ca. 1 mm^2 to decrease current magnitudes. Prior to voltammetry, the PGE electrode surface was polished with 1 μm of alumina (Buehler, U.S.A.), then sonicated thoroughly. An FrdAB protein film was applied by smearing approximately 1 μL of protein solution (~0.1 mM) across the electrode surface using a plastic pipet tip and, after a short incubation time, retracting the excess of protein solution. The coated electrode was then transferred immediately to the cell solution. An Fcc_3 protein film was formed by rotating the PGE electrode at 200 rpm in a 0.4 μM protein solution (~1 mL mixed buffer, pH 7.0) and cycling between 0.241 and −0.759 V versus SHE at 100 mV s^{-1} until the faradaic signal stabilized (~5 min). The PGE electrode with protein film was then transferred to a protein-free cell solution at the appropriate pH.

Voltammetry. All experiments were performed in a Glovebox (Vacuum Atmospheres) under a nitrogen atmosphere (oxygen < 4 ppm). The thermostated electrochemical cell was of all-glass construction, with the main compartment housing the PGE working electrode and platinum wire (surface area = 1−3 mm^2) counter electrode. A sidearm compartment, connected via a Luggin capillary and filled with 0.1 M NaCl, housed the saturated calomel reference electrode (SCE). All potentials are quoted versus the standard hydrogen electrode (SHE) with E_{SCE} = 241 mV versus SHE at 25 °C.[35] The cell was enclosed in a Faraday cage to minimize electrical noise.

Cyclic voltammetry (CV) and square-wave voltammetry (SWV) were recorded using an Autolab electrochemical analyzer (Eco-chemie, Utrecht, The Netherlands) equipped with a PGSTAT20 or PGSTAT30 potentiostat. CV data were recorded in the analogue mode with a fast analogue scan generator (SCANGEN) in combination with either a fast AD converter (ADC750) or the more sensitive electrochemical detection (ECD) module. Effects of uncompensated resistance were minimized by using the positive-feedback iR compensation function of the Autolab analyzer, set at values just below those at which current oscillations appear in cyclic voltammograms.[36] Voltammograms were Fourier-filtered to remove remaining noise, then the background (non-faradaic) current was subtracted using a program (developed by Dr. H. A. Heering and Dr. C. Léger) which fits a cubic spline function[37] to the baseline in regions sufficiently far from the peak, and extrapolates it throughout the peak region.

To determine whether uncompensated resistance had any influence on the measured SWV data and analysis, voltammograms were measured with electrodes having different geometric areas (0.5−3 mm^2) with and without the positive-feedback iR compensation function. For the data acquired (in all cases, currents were <300 μA), some differences were observed when larger areas (3 mm^2) were used without iR compensation. Peak splitting occurred at lower frequencies as

(31) Jeuken, L. J. C.; McEvoy, J. P.; Armstrong, F. A. *J. Phys. Chem. B* **2002**, *106*, 2304−2313.
(32) Gordon, E. H. J.; Pealing, S. L.; Chapman, S. K.; Ward, F. B.; Reid, G. A. *Microbiology* **1998**, *144*, 937−945.
(33) Doherty, M. K.; Pealing, S. L.; Miles, C. S.; Moysey, R.; Taylor, P.; Walkinshaw, M. D.; Reid, G. A.; Chapman, S. K. *Biochemistry* **2000**, *39*, 10695−10701.
(34) Hirst, J.; Armstrong, F. A. *Anal. Chem.* **1998**, *70*, 5062−5071.
(35) Bard, A. J.; Faulkner, L. R. *Electrochemical Methods: Fundementals and Applications*; Wiley: New York, 1980.
(36) Britz, D. *J. Electroanal. Chem.* **1978**, *88*, 309−352.
(37) Press, W.; Flannery, B.; Teukolsky, S.; Vetterling, W. *Numerical Recipes in Pascal*; Cambridge University Press: New York, 1989.

compared to measurements performed with smaller areas and using iR compensation. In the most extreme case, a shift of ~0.3 times the frequency was observed. In the modeling procedure (vide infra), this corresponds to a change in the ET rates of about a factor of 3. We also observed a significant influence on the SWV peak heights, which were much smaller at frequencies >500 Hz when the iR drop was not adequately compensated.

Modeling. General Considerations. Electron-transfer rates were modeled using the Butler−Volmer equations:[35]

$$k_{ox}^{BV} = k_0 \exp\left(\frac{-\alpha nF(E - E^\circ)}{RT}\right) \quad (1a)$$

$$k_{red}^{BV} = k_0 \exp\left(\frac{(1 - \alpha)nF(E - E^\circ)}{RT}\right) \quad (1b)$$

in which E is the applied potential, E° is the formal reduction potential of the adsorbed couple, n is the number of cooperatively transferred electrons, α is the transfer coefficient representing the degree of symmetry (about E°) of the rate constants for oxidation and reduction ($\alpha = 0.5$ for the symmetrical case), and k_0 is the rate at zero overpotential. The terms R, T, and F have their usual meanings.

For a range of protein−protein[38−46] and protein−electrode[31,47−49] systems, the interfacial electron transfer has previously been reported to be limited by a process which is believed to involve motions within the precursor complex that are required to optimize the electronic coupling. The possibility that the ET rates are ultimately limited (gated) in this way was accommodated empirically using the following equation:

$$\frac{1}{k_{ox}} = \frac{1}{k_{ox}^{BV}} + \frac{1}{k_{max}} \quad (2)$$

with k_{max} representing the rate of the reaction preceding ET, and thus limiting the ET rate. An analogous expression with an equal k_{max} value was used to calculate the rate of reduction (k_{red}).

Cyclic Voltammetry. For modeling the CV data, only the FAD was considered since the peak maxima are dominated by this group.

$$FAD_{ox} \underset{k_{ox1}}{\overset{k_{red1}}{\rightleftharpoons}} FAD_{semi} \underset{k_{ox2}}{\overset{k_{red2}}{\rightleftharpoons}} FAD_{red} \quad (3)$$

Initially, the CV data were analyzed in terms of the nonhopping model. To simulate the cooperative two-electron-transfer reaction of the FAD, we made the simplifying assumption that E^0_{FAD1} and E^0_{FAD2} for the reactions $FAD_{ox} \rightleftarrows FAD_{semi}$ and $FAD_{semi} \rightleftarrows FAD_{red}$, respectively, are equal. This corresponds to an apparent cooperativity (n_{app}) ~1.4 and a half-height peak width of 62 mV at 10 °C.[25,50] Furthermore, k_0 was assumed to be the same for both ET reactions (and thus $k_{ox1} = k_{ox2}$ and $k_{red1} = k_{red2}$ at all potentials). Increasing the difference between E^0_{FAD1} and E^0_{FAD2} (≤20 mV) did not significantly change the quality of the fit, although it did influence the k_0 value (<20%). Cyclic voltammograms were calculated using a finite difference procedure[51] based on Butler−Volmer kinetics (eq 1) with a limiting ET rate (eq 2) with the following type of expression to calculate the flux:

$$\frac{d[FAD_{red}]}{dt} = -k_{ox2} \times [FAD_{red}] + k_{red2} \times [FAD_{semi}] \quad (4)$$

Experimental results were fit by a Levenberg−Marquardt procedure,[52] in which the error of the experimental peak positions was estimated to be ±5 mV.

Even at the slowest scan rates, voltammograms of FrdAB display a small, nonideal separation between oxidative and reductive peaks. This peak separation is observed for a range of proteins and might be due to slowly interconverting redox-dependent orientations of the protein on the electrode.[28,34,53] In this paper, we have added a small (~10 mV), constant peak separation to the simulated data of FrdAB to compensate for this nonideality.

Square-Wave Voltammetry. A finite difference procedure[51] was also used to model the SWV data. For simplification, the redox chain was treated as an integral entity with a single value of E°, k_0, and k_{max}, and it was assumed that redox equilibrium within the redox chain was maintained throughout. Consequently, the current due to the redox chain could be calculated by multiplying the current modeled for a single redox-chain component by the number of redox groups in the chain (see also Figure 4). For the nonhopping model, the Butler−Volmer equations with a maximum ET rate (eqs 1 and 2) were used to calculate the ET rates between the electrode and the redox chain or the FAD group. For the hopping model, the ET rate between the electrode and the redox chain was again calculated using eqs 1 and 2, while the ET rates between the redox chain and the FAD,

$$FAD_{ox} + \text{redox−chain}_{red} \underset{k_{-1}}{\overset{k_1}{\rightleftharpoons}} FAD_{semi} + \text{redox−chain}_{ox} \quad (5a)$$

$$FAD_{semi} + \text{redox−chain}_{red} \underset{k_{-2}}{\overset{k_2}{\rightleftharpoons}} FAD_{red} + \text{redox−chain}_{ox} \quad (5b)$$

had to be consistent with the difference in reduction potential between the redox chain and the FAD, that is,

$$k_1/k_{-1} = \exp\left[\frac{(E^0_{FAD1} - E^0_{redox-chain})F}{RT}\right] \quad (6a)$$

$$k_2/k_{-2} = \exp\left[\frac{(E^0_{FAD2} - E^0_{redox-chain})F}{RT}\right] \quad (6b)$$

The fluxes were then calculated using formulas of the type:

$$\frac{d[FAD_{ox}]}{dt} = \langle -k_1 \times [\text{redox−chain}_{red}] \times [FAD_{ox}] \rangle + \langle k_{-1} \times [\text{redox−chain}_{ox}] \times [FAD_{semi}] \rangle \quad (7)$$

Again, to simulate the cooperative ET reaction of the FAD, we used the simplifying assumption that $E^0_{FAD1} = E^0_{FAD2}$. For the nonhopping model, we assumed that k_0 values for the two one-electron reactions were equal, while for the hopping model we assumed $k_1 = k_{-2}$.[54] Like the CV data, the SWV data were fit by a Levenberg−Marquardt procedure,[52] with the error of the SWV peak positions estimated to be ±10 mV. Also, for the SWV simulations, it was found that increasing

(38) Moser, C.; Dutton, P. L. *Biochemistry* **1988**, *27*, 2450−2461.
(39) McLendon, G.; Pardue, K. *J. Am. Chem. Soc.* **1987**, *109*, 7540−7541.
(40) Zhou, J.; Kostić, N. *J. Am. Chem. Soc.* **1993**, *115*, 10796−10804.
(41) Ivković-Jensen, M. M.; Ullmann, G. M.; Crnogorac, M. M.; Ejdebäck, M.; Young, S.; Hansson, O.; Kostić, N. M. *Biochemistry* **1999**, *38*, 1589−1597.
(42) Qin, L.; Kostić, N. *Biochemistry* **1994**, *33*, 12592−12599.
(43) Ubbink, M.; Ejdebäck, M.; Karlsson, B. G.; Bendall, D. S. *Structure* **1998**, *6*, 323−335.
(44) Amsterdam, I.; Ubbink, M.; Jeuken, L. C.; Verbeet, M. P.; Einsle, O.; Messerschmidt, A.; Canters, G. *Chem.-Eur. J.* **2001**, *7*, 2398−2406.
(45) Pletneva, E. V.; Fulton, D. B.; Kohzuma, T.; Kostić, N. M. *J. Am. Chem. Soc.* **2000**, *122*, 1034−1046.
(46) Davidson, V. L. *Biochemistry* **2000**, *39*, 4924−4928.
(47) Avila, A.; Gregory, B. W.; Niki, K.; Cotton, T. M. *J. Phys. Chem. B* **2000**, *104*, 2759−2766.
(48) Feng, Z.; Imabayashi, S.; Kakiuchi, T.; Niki, K. *J. Chem. Soc., Faraday Trans.* **1997**, *93*, 1367−1370.
(49) Chi, Q.; Zhang, J.; Andersen, J.; Ulstrup, J. *J. Phys. Chem. B* **2001**, *105*, 4669−4679.
(50) Plichon, V.; Laviron, E. *J. Electroanal. Chem.* **1976**, *71*, 143−156.
(51) Britz, D. *Digital Simulation in Electrochemistry*; Springer-Verlag: Berlin, 1988; Vol. 2.
(52) Press, W. H.; Teukolsky, S. A.; Vetterling, W. T.; Flannery, B. P. *Numerical Recipes in C*, 2nd ed.; Cambridge University Press: Cambridge, 1992.
(53) Jeuken, L. J. C.; Armstrong, F. A. *J. Phys. Chem. B* **2001**, *105*, 5271−5282.

(54) It was assumed $k_1 = k_{-2}$ because these values are rate-limiting for very crossed potentials (i.e., large negative difference between $E^{0'}_{FAD1}$ and $E^{0'}_{FAD2}$), since the k_{-1} and k_2 values become very large.

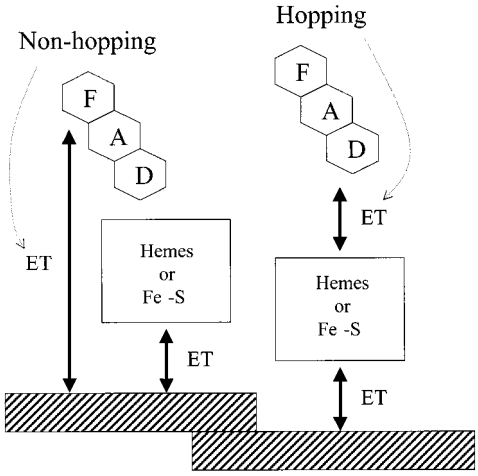

Figure 4. Representations of the nonhopping and hopping models based on which of the CV and SWV is fitted as described in the text.

the difference between E^0_{FAD1} and E^0_{FAD2} ($\leq$20 mV) did not significantly alter the quality of the fit, but did change the determined values of k_0 or k_1 ($=k_{-2}$) (<20%).

To account for the sampling time required by the potentiostat to measure the current at the end of the period, the current in the simulations was averaged from the start until the end of the sampling period. Calculations showed that introduction of the sampling time into the model significantly influenced the simulation and therefore needed to be included.

Results

Modeling. Throughout this paper, we will analyze the forward and backward currents of the SWV separately, and we will not comment on the net current since this is the difference of the former two currents and does not provide additional information. We will further denote the reductive currents (measured after a negative step in potential within the square-wave voltammetry sequence) as the backward currents, and the oxidation signals as forward currents (see Figure 3).

Peak Splitting. Figure 5 shows the results of several SWV simulations, in which the peak positions of the forward and backward current are plotted against frequency. First, we will discuss the case of a single ET site (Figure 5A). At high frequencies (*f*), the forward and backward currents show identical (but oppositely signed) peaks, positioned at $E°$.[55] At low *f*, the peaks separate, approaching a maximum splitting of $2 \times E_{sw}$. As explained elsewhere,[31,56,57] this peak splitting is a consequence of the way that the ET rate to or from the redox site increases with overpotential (as modeled with the Butler–Volmer eq 1). In SWV, the current is sampled at the end of each period (see Figure 3); importantly, *at long periods* (low *f*), a fast ET reaction will already be complete, and no current will be detected. At potential values close to $E°$, the E_{sw} steps will result in the current being sampled at high overpotentials ($E° \pm E_{sw}$), where both reduction and oxidation are fast. However, when the voltammogram is measured at $E° \pm E_{sw}$, the E_{sw} steps in one-half of the cases (reduction or oxidation) result in the current being measured at zero overpotential ($E = E°$), that is, at *lower* reduction or oxidation rates, and a current may be detected. At low *f*, this results in peaks being detected at $E° \pm E_{sw}$ (and thus the peak splitting is $2 \times E_{sw}$). Whether or not peak splitting occurs will depend on the values of *f* and E_{sw} used in the SWV and on the ET rates as a function of overpotential.

For a range of protein–protein[38–46] and protein–electrode[47–49] systems, it has been found that intermolecular or interfacial ET is limited (gated) by a preceding process. The nature of this restriction on rates is not yet clearly defined, but it is believed to involve adjustments in the configuration of the precursor complex required to optimize electronic coupling.[38–48] This limitation of the ET rate shows up profoundly in the SWV results, as described recently for the small electron-transfer protein, azurin.[31] Figure 5A shows that SWV is indeed very sensitive to the limitation in ET rate (with the rate, k_{max}, modeled by eq 2).

Multicenter Enzymes. Referring to the fumarate reductases studied in this paper, Figure 5 also shows the results for a two-component system that includes a redox chain (with three one-electron redox groups) and a two-electron-transfer group (i.e., the FAD with $n_{app} = 1.4$). As in the first example, this modeled system includes limited ET rates at high overpotentials. The two ET mechanisms we have outlined in the Introduction are represented in Figure 4. For both models, the effect of varying two parameters is analyzed. The first parameter is the difference between the reduction potential of the redox chain and the FAD, and we note that this difference can be systematically varied in the experiments by altering the pH (the FAD potential is much more pH-dependent than the redox-chain components). The second parameter is the ET rate to the FAD, which, for the nonhopping model, can be determined from cyclic voltammetry experiments.

Nonhopping Model. In Figure 5B and C, the electrons are transferred directly to the FAD via a nonhopping mechanism (Figure 4, left). While this need not be the case, the examples shown here are for the case in which the ET to the redox chain is faster than that to the FAD, which is in line with our results for FrdAB and Fcc_3 (see later). When the $E°$ value of the redox chain is equal to that of the FAD, little difference is seen as compared to a system that contains only one redox group (Figure 5A). However, when the $E°$ values differ relative to one other, the average peak position shifts with frequency. At high frequencies (short periods), the faster ET to the redox chain results in higher currents as compared to those of the slower ET to the FAD (see Figure 3). At lower frequencies (longer periods), the redox chain will already be at equilibrium with the electrode by the time the current is sampled (at the end of the period). The slower ET to the FAD will not yet be at equilibrium and, consequently, will be the sole contributor to the current measured (Figure 3). In the nonhopping model, the FAD transfers electrons directly with the electrode, and, therefore, the ET rate to the FAD will have a similar dependency on potential as a protein with a single redox site. Because the FAD is the sole contributor to the signals at low frequencies, the SWV simulation at low frequencies is identical to that of the model with a single redox site (as shown in Figure 5A), and thus the peak splitting approaches $2 \times E_{sw}$. Consequently, the average of the peak positions at low frequency in Figure

(55) At even higher *f* (or lower k_0), the peak maxima will deviate from $E^{0\prime}$ (see refs 56,57). Because our measurements are limited to <2000 Hz and our ET rates are fast ($k_0 > 100\ s^{-1}$), this region is not relevant and will, therefore, not be discussed in our modeling section.

(56) O'Dea, J. J.; Ribes, A.; Osteryoung, J. G. *J. Electroanal. Chem.* **1993**, *345*, 287–301.
(57) Reeves, J.; Song, S.; Bowden, E. *Anal. Chem.* **1993**, *65*, 683–688.

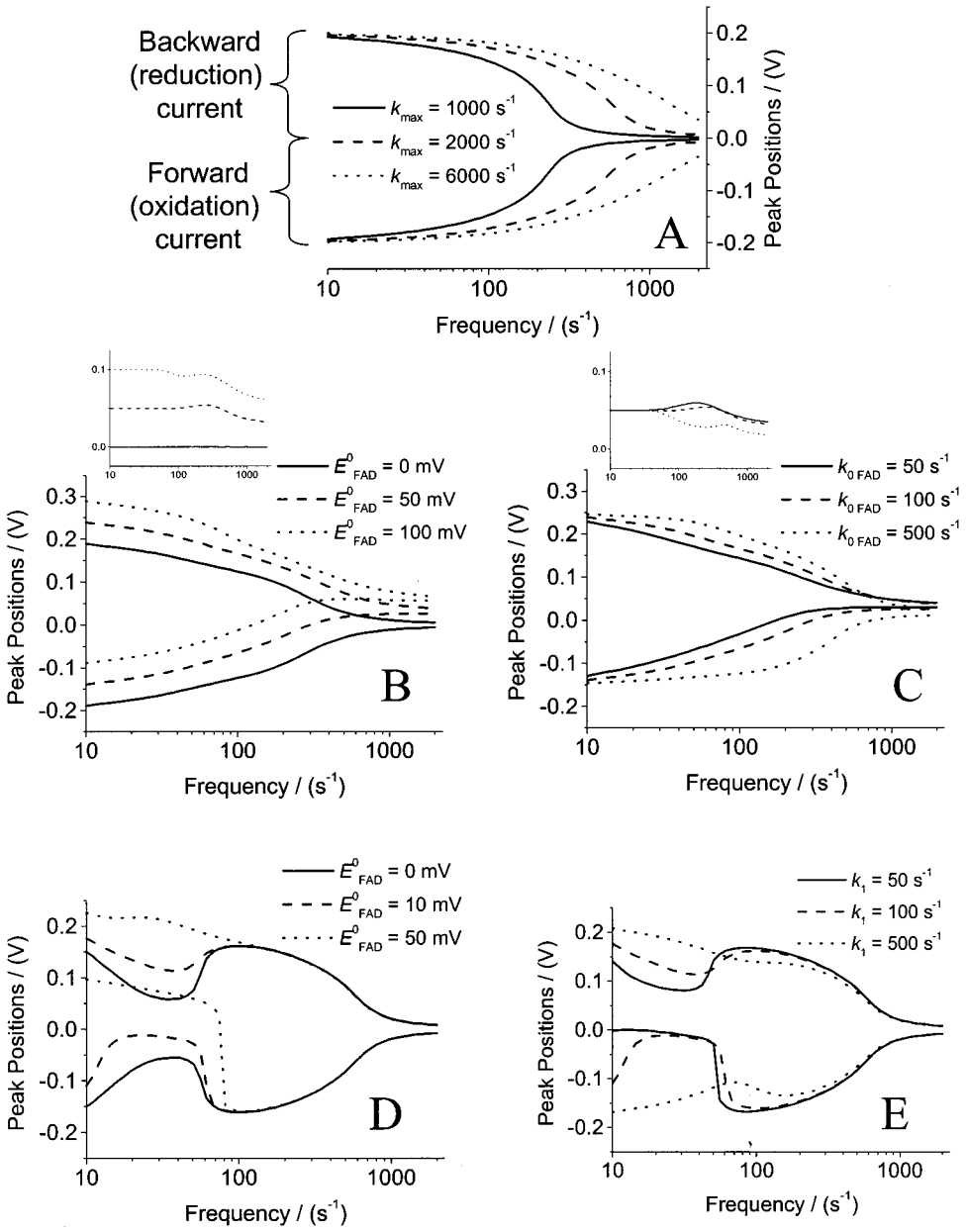

Figure 5. SWV simulations (forward and backward peak positions as a function of frequency) with E_{sw} = 0.2 V. If the simulated SWV contains two resolved peaks, the peak position of the highest peak is shown. (A) A single ET site with $E°$ = 0 V, k_0 = 500 s^{-1}, and k_{max} as indicated. (B and C) Multicenter enzyme with one FAD group and three identical, one-electron centers in the redox chain, with ET occurring via a nonhopping mechanism (see Figure 4, left model). In both cases, $E^0_{redox-chain}$ = 0 V, $k_{0\ redox-chain}$ = 500 s^{-1}, and k_{max} = 2000^{-1}. For (B), $k_{0\ FAD}$ = 100 s^{-1} and for (C), E^0_{FAD} = 0.05 V. Insets show the average peak positions of forward and backward peaks. (D and E) Multicenter enzyme as before but occurring via a hopping mechanism (see Figure 4, right model). In both cases, $E^0_{redoxchain}$ = 0 V, $k_{0\ redoxchain}$ = 500 s^{-1}, and k_{max} = 2000 s^{-1} and for (D), $k_{redoxchain \rightarrow FAD} = k_1$ = 100 s^{-1}. For (E), E^0_{FAD} = 0.01 V.

5B and C is given by the reduction potential of the FAD, while at higher frequency the average of the peak positions is dependent on the reduction potential of both the FAD and the redox chain. Where and how the transition of average peak positions takes place depend on the ratio of the ET rates of the two components (Figure 5C).

Hopping Model. In the hopping mechanism, the electrons are transferred first to the redox chain, then relayed on to the FAD (Figure 4, right), which results in "Jellyfish"-shaped plots (Figure 5D and E). Analogous to the nonhopping mechanism, the FAD signal dominates at low frequency. Contrary to the hopping mechanism, the ET rate to the FAD depends on the intramolecular rate constants and the oxidation state of the groups involved (eq 5). Because of this difference, the peak splitting of the FAD at a certain frequency is less than that for the redox chain, which results in a "constriction" in the plot that coincides with the frequency at which the FAD signal becomes resolved. The constriction is present as long as the intramolecular ET between the redox chain and the FAD is slower than the interfacial exchange between the electrode and the redox chain ($k_1 < k_{max}$). Unlike the nonhopping model, the peak splitting does not approach 2 × E_{sw} (unless $k_1 \geq k_{0\ redoxchain}$). Furthermore, when the $E°$ value of the redox chain is different from that of the FAD, the simulations show a pronounced asymmetry (Figure 5E). The difference in $E°$ (=(RT/nF) × ln(K_d)) results in a difference between the forward and

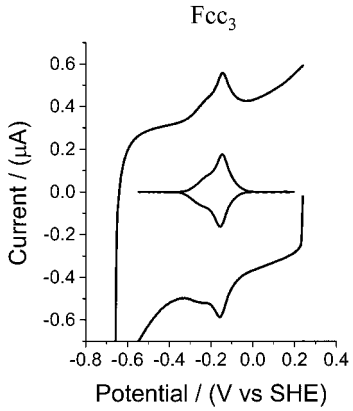

Figure 6. Cyclic voltammogram (raw data and smoothed baseline-subtracted signal) of Fcc_3 (mixed buffer, pH 7.0, 200 μg mL^{-1} polymyxin, 10 °C, scan rate = 100 mV s^{-1}, electrode area = 3 mm^2).

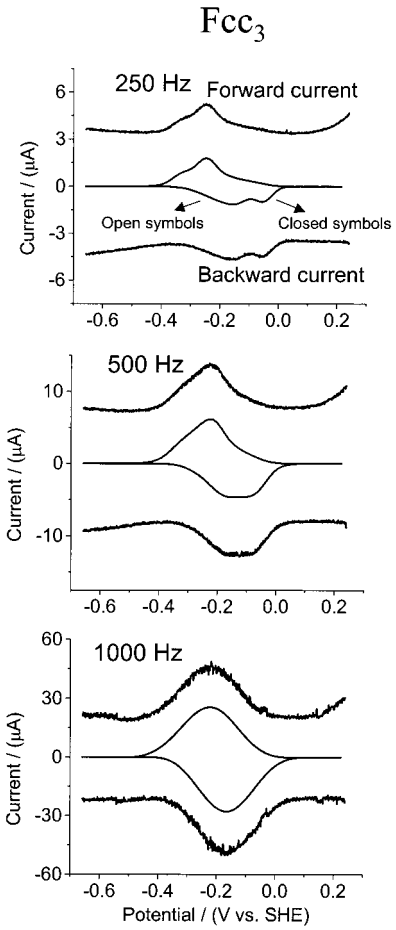

Figure 7. Square-wave voltammograms (raw data and smoothed baseline-subtracted signals) of Fcc_3 at several frequencies (mixed buffer, pH 7.0, 200 μg mL^{-1} polymyxin, 10 °C, E_{sw} = 125 mV, electrode area ≈ 0.8 mm^2).

backward rate constants, which manifests itself in a profound change in the average peak positions as compared to the $E°$ of either the redox chain or the FAD.

Experiments. Fcc_3. Figure 6 shows a cyclic voltammogram (CV) from an Fcc_3 film at pH 7.0. Typically, the coverage, as estimated from the area under the peaks and using the geometric area of the electrode, is 9−13 pmol cm^{-2}. After baseline subtraction, the envelope consists of a broad base resulting from the redox transitions of the four hemes upon which the sharper signal of the two-electron transition of the FAD is superimposed.[23,24] While the reduction potential of the FAD is pH-dependent (30−60 mV/pH unit for 6 ≤ pH ≤ 8), the heme envelope is largely uninfluenced by pH.[23]

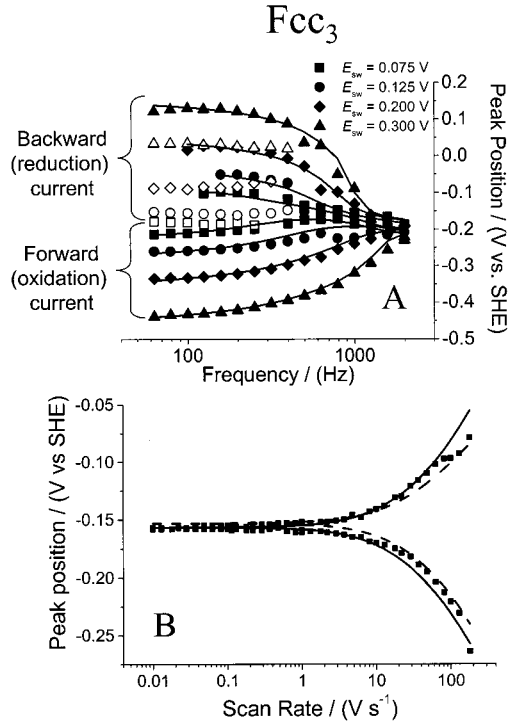

Figure 8. (A) Peak positions of forward and backward currents of square-wave voltammograms of Fcc_3 (mixed buffer, pH 7.0, 200 μg mL^{-1} polymyxin, 10 °C) at four different values of E_{sw} plotted against frequency (log scale). Lines represent simulations as discussed in the text. Open and closed symbols are as denoted in Figure 7. (B) Peak positions as a function of scan rate (log scale) for cyclic voltammograms of Fcc_3 (mixed buffer, pH 7.0, 200 μg mL^{-1} polymyxin, 10 °C). The lines represent simulations (solid line: simulation using FAD group only with k_0 = 970 s^{-1}. Dashed line: simulation using nonhopping model represented in Figure 4(left)), with parameters shown in the second line of Table 1. According to the CV measurements, the reduction potentials of the hemes span about 80 mV. Thus, simulations treating the hemes as identical centers result in peaks that are too narrow. To correct for this, the n value for each of the hemes was set to 0.5 (which gives a half-height peak width of 172 mV[30]).

Figure 7 shows SWV results from an Fcc_3 film. The results obtained at pH 6.0, 7.0, and 8.0 were very similar, and the peak positions for a range of switching amplitudes (E_{sw}) are plotted against frequency in Figure 8A. At high frequency, the forward and backward peaks do not have a sharp and resolved FAD feature as observed in the CV at 100 mV s^{-1} (Figures 6 and 7). However, when the frequency is lowered, a sharper signal appears. At lower frequencies, two peaks can be observed for the backward current (one sharp and one broad peak, see Figure 7). For the forward current, only one peak maximum is observed, since the sharp peak lies on top of the broad peak. For reasons discussed later, only the sharp peaks will be considered (closed symbols). The forward and backward peaks are relatively unseparated at high frequency, while at lower frequency the peak splitting approaches 2 × E_{sw}.

Comparison with the CV data strongly suggests that the FAD is responsible for the sharper peaks in the SWV. Figure 9 gives the average peak potentials as a function of frequency for three different pH values; these provide compelling evidence that the sharper signals indeed belong to the FAD. At lower frequencies, the average potential of the sharp peaks (closed symbols) coincides exactly with the reduction potential of the FAD

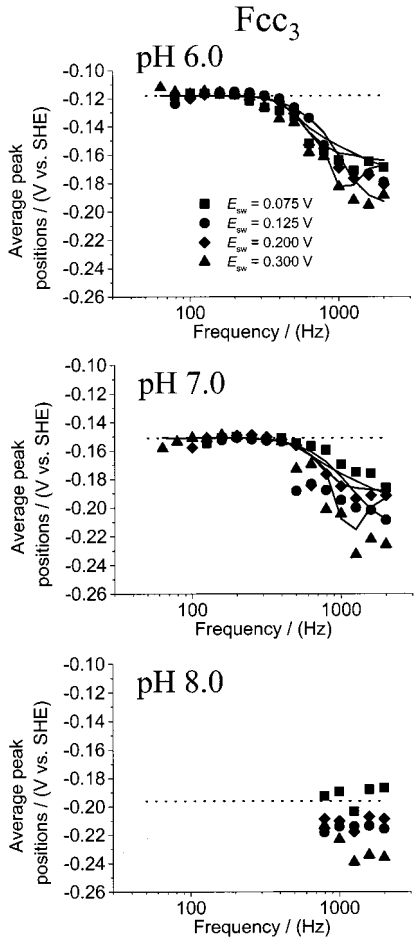

Figure 9. Average peak positions of sharp signals (see Figure 7) of forward and backward currents from square-wave voltammograms of Fcc_3 (mixed buffer, 200 μg mL^{-1} polymyxin, 10 °C) plotted against frequency (log scale) for four different E_{sw} and three pH values. Lines represent simulations as discussed in the text. Dotted lines show $E^{0'}_{FAD}$ determined from CV under identical conditions.

($E^{0'}_{FAD}$) determined by CV (Figure 9, dotted lines). Because the sharp peak is unresolved in the backward current at pH 8.0, no average peak potential can be given. However, assuming that at pH 8.0 the peak splitting also approaches 2 × E_{sw} at low frequency, the potential of the sharper peaks also corresponds with $E^{0'}_{FAD}$ at pH 8.0 (data not shown). $E^{0'}_{FAD}$ depends strongly on pH,[23] and, as expected, so does the average of the sharper peaks. In contrast, the average potential of the forward and backward peaks measured at higher frequencies does not coincide with $E^{0'}_{FAD}$ and is relatively independent of pH. This suggests that the signal intensity arises mainly from the heme groups with the FAD undistinguished. There is no evidence for a constriction as observed for FrdAB (see below).

FrdAB. Figure 10 shows a cyclic voltammogram of FrdAB. As for Fcc_3, the electrochemical response of FrdAB can be deconvoluted into signals due to the redox chain and signals due to the FAD. The coverage (typically 3−8 pmol/cm^2) is somewhat lower than that for Fcc_3, and the reduction potential of one of the redox groups of FrdAB ($[4Fe-4S]^{2+/+}$) lies outside the envelope of the remaining redox groups. The $[4Fe-4S]^{2+/+}$ cluster is also visible in the square-wave voltammograms when measured with low E_{sw} values, but at higher E_{sw} the signal disappears under the envelope of the other redox groups (backward current) or moves out of the scan range (forward

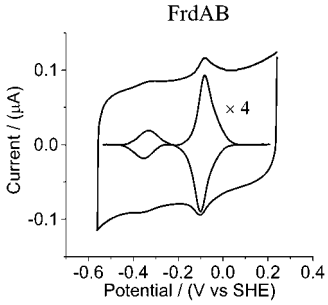

Figure 10. Cyclic voltammogram (raw data and smoothed baseline-subtracted signal (current is multiplied × 4) of FrdAB (mixed buffer, pH 8.0, 200 μg mL^{-1} polymyxin, 10 °C, 20% glycerol, scan rate = 100 mV s^{-1}, electrode area ≈ 1 mm^2).

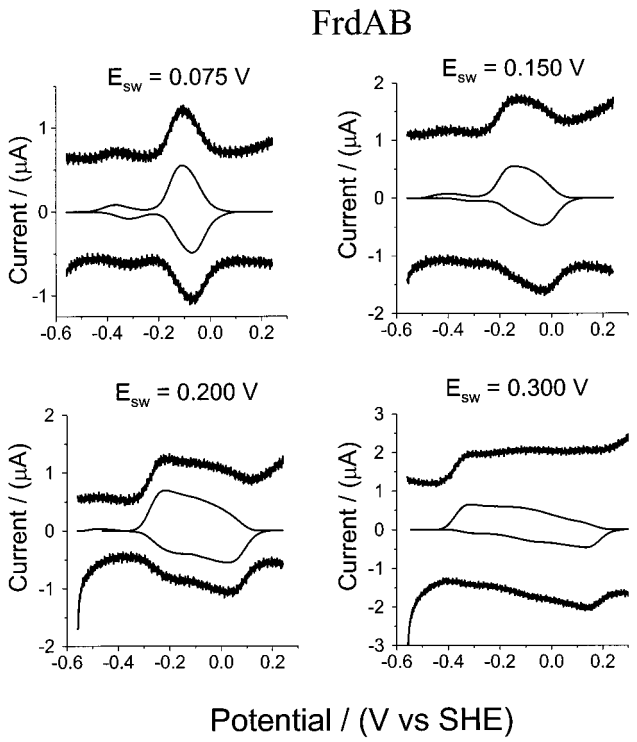

Figure 11. Square-wave voltammograms (raw data and smoothed baseline-subtracted signals) of FrdAB at four different E_{sw} (mixed buffer, pH 8.0, 200 μg mL^{-1} polymyxin, 10 °C, 20% glycerol, f = 31 Hz, electrode area ≈ 1.0 mm^2). From the voltammograms at E_{sw} = 0.2 and 0.3 V, a constant current has been subtracted from the raw data for clarity (1.5 and 2.0 μA, respectively).

current) (Figure 11). Similarly to Fcc_3, two observations show that the square-wave voltammograms of FrdAB are dominated by FAD signals at lower frequencies, while at higher frequencies the Fe−S clusters seem to be dominant. First, although at low frequency (and low E_{sw}) the $[4Fe-4S]^{2+/+}$ signal is small relative to the major peak (see Figure 11), at high frequency the $[4Fe-4S]^{2+/+}$ signal becomes more intense (approximately one-half that of the major peak, data not shown). Second, like Fcc_3, the average of the major peaks at low frequency corresponds to the pH-dependent reduction potential of the FAD (Figure 12). The signals from the $[4Fe-4S]^{2+/+}$ cluster will not be analyzed further in this paper since they are only visible with low E_{sw} values, while the measurements at higher E_{sw} values are a vital part of the analysis.

Importantly, there are two main differences between the results observed for FrdAB and those obtained with Fcc_3. The first is that the FAD signal becomes dominant at lower

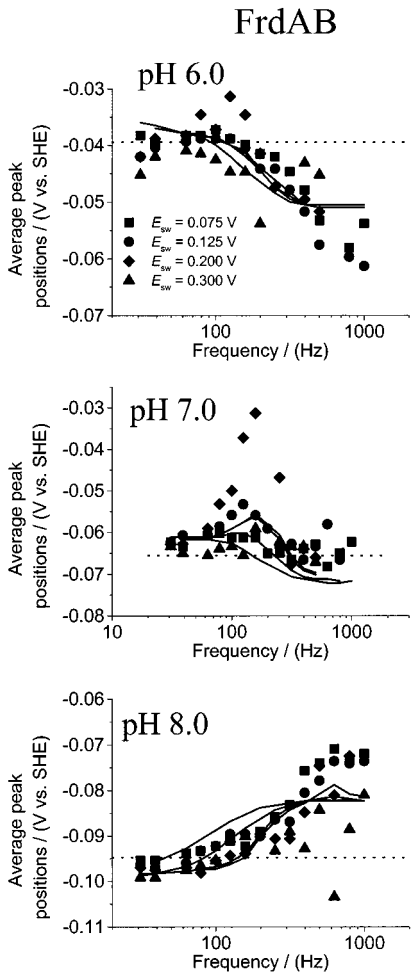

Figure 12. Average peak positions of forward and backward currents of square-wave voltammograms of FrdAB (mixed buffer, 200 μg mL^{-1} polymyxin, 10 °C, 20% glycerol) at four different E_{sw} and three pH values, plotted against frequency (log scale). Lines represent simulations as discussed in the text. Dotted lines show $E^{0'}_{FAD}$ determined from CV under identical conditions.

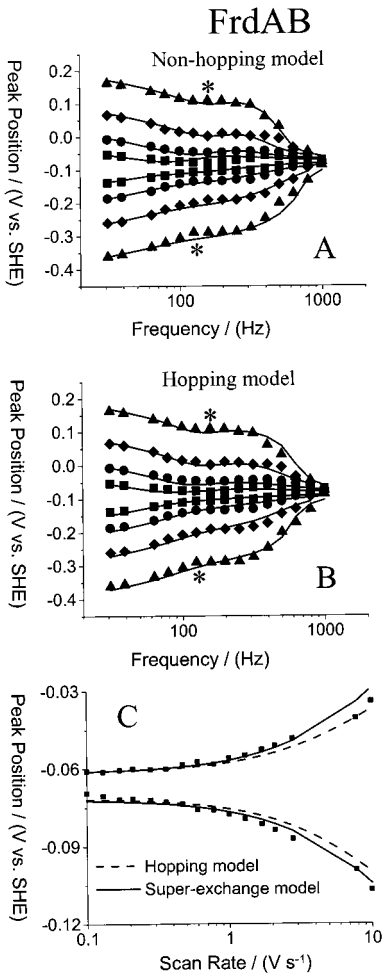

Figure 13. (A and B) Peak positions of forward and backward currents of square-wave voltammograms of FrdAB (mixed buffer, pH 8.0, 200 μg mL^{-1} polymyxin, 10 °C, 20% glycerol) at four different E_{sw}, plotted against frequency (log scale). The "*" symbol indicates the observed "constrictions" in the peak splitting. (C) Peak positions of cyclic voltammograms of FrdAB plotted against scan rate (log scale). The lines represent simulations as discussed in the text.

frequencies for FrdAB than for Fcc_3 (~100 vs ~500 Hz, respectively, see Figures 9 and 12). The second difference becomes most clear at pH 8.0 (Figure 13A and B), where, instead of a continuous increase in peak splitting with decreasing frequency, the FrdAB data exhibit a constriction (denoted with a *) resulting in the Jellyfish-shaped plot.

Discussion

The fact that the FAD signals in the SWV data are not resolvable at higher frequencies but dominate the envelope at lower frequencies means that ET to and from the FAD is slower than interfacial ET to and from the redox chain. This is not surprising since in both Fcc_3 and Frd the active site FAD is the most buried redox group in the protein, as shown in Figure 14. In this figure, the distances between the redox groups and the protein surfaces are presented, in which the solvent-excluded surfaces[58] are calculated for increasing probe sizes. It is apparent that a large flat electrode surface would not be able to move closer than ~15 Å to the FAD groups, while the relatively fast ET kinetics suggest better electronic couplings than are expected for such distances.[1] This implies that the redox chain is necessary for fast electron transfer between the electrode and the FAD.

Although the SWV data of Fcc_3 and Frd show some explicit and distinguishing features, the complex nature of the enzymes required us to incorporate several simplifications into the models that were used to simulate the data. As explained in the Results section, two limiting cases have been considered, that is, the hopping and the nonhopping models (see Figure 4). We will now summarize the simplifications and assumptions made for both models.

(i) By analogy with the small protein azurin, described previously,[31] electron transfer from the electrode to the proteins is described by the Butler−Volmer equation but is limited or gated by a physical process (eqs 1 and 2), which is the same for reduction and oxidation.

(ii) Simulations of the FrdAB data do not include the [4Fe−4S]$^{2+/+}$ cluster, which has a reduction potential that is very different from those of the other centers. Assuming electrons are distributed rapidly and thermodynamically among the Fe−S clusters, this simplification is justified (except that the signal due to the [4Fe−4S]$^{2+/+}$ cluster will not be present in the simulations). The remaining redox centers in the chains are

(58) Sanner, M. F.; Olson, A. J.; Spehner, J. C. *Biopolymers* **1996**, *38*, 305−320.

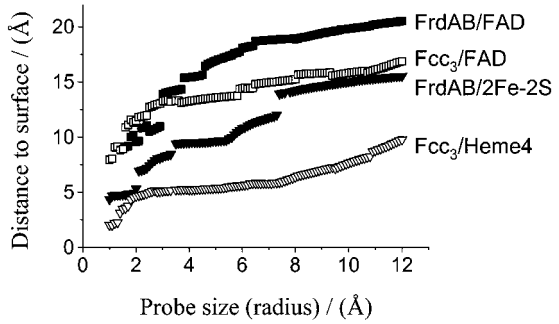

Figure 14. Minimum distances between four redox groups and the solvent-excluded surfaces of FrdAB and Fcc_3 at various probe sizes as calculated by the program MSMS[58] (freely available at http://www.scripps.edu/~sanner/python/). For the FAD molecules, only the isoalloxazine groups were used to calculate the distances to the surfaces. The crystal structures are taken from Brookhaven Data Bank 1QJD[21] and 1FUM[22]) with the two domains (FrdC and D) deleted from the PDB file of the Frd crystal structure (FrdABCD) to obtain FrdAB. The solvent-excluded surface is determined by the probe sphere tangential to the surface atoms of the proteins.[58,65] Therefore, the electrode surface could be seen as analogous to the probes (with probe size > 10 Å) and the minimum distance being the distance between the FAD, 2Fe−2S cluster, Heme 4 and the electrode surface. The 2Fe−2S cluster and Heme 4 are the redox groups in the chains which are closest to the FAD in FrdAB and Fcc_3, respectively.

treated as being identical (equal $E°$, k_0, and k_{max}) with an equal dependence of ET rate on potential. Together with the assumption that ET among the groups in the redox chain is fast, this allows a simplification of the model so that all redox groups in the chain can be represented by a single component (see Figure 4; the current contribution calculated for a single redox group is multiplied by the number of groups in the chain). Calculations in which each redox group in the chain is treated individually were performed to check the validity of this approximation. These calculations showed no significant improvement of the fit.

(iii) The reduction potentials of the two one-electron reactions of the FAD as well as the rates of the two reactions (either k_0 or k_1 and k_{-2}) are assumed to be equal (giving an $n_{app} = 1.4$). Both assumptions are realistic; n_{app} is close to the measured value of 1.60 ± 0.12 (see ref 23), and the trumpet plots (Figures 8B and 13C) are symmetric, indicating that the reduction and oxidation rates of the FAD are similar. Furthermore, calculations showed that small deviations (<20 mV) in $E^{0'}_{FAD1}$ and $E^{0'}_{FAD2}$ (with $[E^{0'}_{FAD1} + E^{0'}_{FAD2}]/2$ remaining the same) did not influence the qualities of the fits.

(iv) In the hopping model, it is assumed that the ET rates from the redox chain to the FAD can be approximated by a "redox-state level" dependence as shown in eq 7.

(v) Finally, it is assumed that (the pulsed nature of) the electrode potential does not influence the intramolecular ET or that intramolecular ET does not give rise to a strong capacitative (nonfaradaic) current. This latter assumption is well supported by our previous work on protein film voltammetry.[28,29]

Simulations of Fcc_3 Data. For Fcc_3, the SWV results shown in Figure 8 provide compelling evidence for a ET mechanism that does not require hopping via the heme groups. Electron transfer to and from the FAD group is simply described in terms of the Butler−Volmer model with a maximum rate constant representing the limitation of the preceding reactions on the ET rate. The lines in Figures 8A and 9 show the results of the best fits using the nonhopping model that is represented in Figure 4 (left). For the FAD group, $E^{0'}$ and k_0 values were used that were independently determined from (fast scan) CV data (Figure 8B, solid line). The ET rate to the FAD was assumed to be limited by the same process that limits the ET rate to the hemes and thus to have the same value for k_{max}.[59] The parameters acquired from the fits are presented in Table 1. Although k_0 values for the FAD were used that were independently determined by fast scan CV, the SWV data could also be fit without fixing the value for k_0. In the latter case, k_0 values were obtained that were similar (±50%) to those obtained by CV (data not shown). Furthermore, when this SWV model, which included the redox chain, was used to simulate the CV data, a good fit was obtained (Figure 8B, dashed line).

Simulations of FrdAB Data. The most important differences between the experimental results for FrdAB and Fcc_3 are as follows: (i) A constriction is clearly observed in the plots of potential against frequency (denoted with a "*" symbol in Figure 13A and B). This constriction is seen because the peak splitting of the FAD group is smaller than that of the Fe−S clusters, and at <300 Hz the FAD signals become resolved above the redox-chain signals (and vice versa). (ii) The difference in average peak position at low versus high frequency (i.e., the FAD group versus the redox chain) never exceeds 30 mV for FrdAB, while for Fcc_3 there is a 80 mV shift at pH 6.0 (Figures 9 and 12).

The FrdAB data could only be simulated by the nonhopping model if two different maximum ET rates (two k_{max} values, one for the redox chain and one for the FAD) were used (Figure 13A, for parameters see Table 2; this model has not been considered in the Modeling section). As before, k_0 for the FAD group was independently determined with CV (Figure 13C). Importantly, and in contrast with Fcc_3, the FrdAB data could be modeled well with a hopping mechanism (Figures 4 (right) and 13B; for parameters see Table 3). Within the hopping model, the ET rate constants to and from the FAD could not be determined independently from the CV data, since the peak positions in the CV depend on a combination of parameters. However, reasonable fits of the CV data are obtained using the parameters determined from the SWV data (Figure 13C, dashed line).

Comparison between Fcc_3 and Frd. On the basis of the results from FrdAB simulations, it is important to rationalize why the Fcc_3 data could not be described with a hopping model. The first reason is that all simulations based on a hopping ET mechanism result in Jellyfish shapes such as those observed for FrdAB (Figure 13A and B) but not for Fcc_3 (Figure 8A). The second reason is that when the reduction potentials of the redox chain and the FAD groups lie far apart, the forward and backward rates from the FAD to the redox chain differ by orders of magnitude, and, consequently, ET to the FAD is fast, while ET from the FAD back to the electrode is very slow (or vice versa). This would result in a profoundly asymmetric response in the SWV data when peak positions are plotted against frequency (Figure 5D and E), a feature that is *not* observed in the data (Figure 8A). In other words, the difference of up to 80 mV between high and low frequency observed in the Fcc_3 data makes it impossible to simulate these data with a hopping model.

Attempts were made to fit the Fcc_3 SWV data with a model based on a hopping mechanism in which all the redox groups

(59) Modeling the data with different k_{max} values for the hemes and the FAD did not significantly improve the fits.

Table 1. ET Parameters for Fcc_3 Obtained by Fitting SWV Data with a Nonhopping Mechanism

	$k_{0(FAD)}$[a] (s^{-1})	$k_{0(hemes)}$ (s^{-1})	k_{max} (s^{-1})	$E^{0'}_{FAD}$[c] (mV vs SHE)	$E^{0'}_{hemes}$ (mV vs SHE)
pH 6.0	1090 ± 140	4000 ± 200	5400 ± 100	−0.118	−0.214 ± 0.004
	1570 ± 100	3800 ± 200	5300 ± 200	−0.118	−0.210 ± 0.005
pH 7.0	970 ± 190	4900 ± 300	6000 ± 200	−0.151	−0.235 ± 0.005
	1550 ± 110	4200 ± 300	5600 ± 200	−0.151	−0.232 ± 0.005
pH 8.0	190 ± 30[b]				
	890 ± 60	3700 ± 300	5200 ± 200	−0.196	−0.230 ± 0.008

[a] The first line (including error) at each pH is independently determined using CV and consequently fixed in the fitting procedures for the SWV. For the second line at each pH, k_0 is allowed to optimize freely, and the error is determined from the fitting procedure of the SWV data. [b] No good fit could be obtained for the SWV data while fixing this value to that obtained from CV experiments. [c] Values determined from CV and fixed in the fitting procedure of the SWV data.

Table 2. ET Parameters for FrdAB Obtained by Fitting Two Sets of SWV Data with a Nonhopping Mechanism

	$k_{0(FAD)}$[a] (s^{-1})	$k_{max(FAD)}$ (s^{-1})	$k_{0(Fe-S)}$ (s^{-1})	$k_{max(Fe-S)}$ (s^{-1})	$E^{0'}_{FAD}$[a] (mV vs SHE)	$E^{0'}_{Fe-S}$ (mV vs SHE)
pH 6.0	330 ± 50	1100 ± 100	750 ± 100	2900 ± 100	−0.039	−0.065 ± 0.005
pH 7.0	280 ± 40	1100 ± 100	1300 ± 100	3100 ± 100	−0.065	−0.068 ± 0.007
pH 8.0	130 ± 20	900 ± 100	460 ± 30	2600 ± 100	−0.093	−0.068 ± 0.004

[a] Values are independently determined from CV and used to model SWV.

Table 3. ET Parameters for FrdAB Obtained by Fitting Two Sets of SWV Data with a Hopping Mechanism

	$k_{(Fe-S\rightarrow FAD)} = k_1$ (s^{-1})	$k_{0(Fe-S)}$ (s^{-1})	k_{max} (s^{-1})	$E^{0'}_{FAD}$[a] (mV vs SHE)	$E^{0'}_{Fe-S}$ (mV vs SHE)
pH 6.0	1200 ± 100	450 ± 40	3700 ± 300	−0.039	−0.050 ± 0.003
pH 7.0	1300 ± 100	900 ± 100	2600 ± 100	−0.065	−0.067 ± 0.002
pH 8.0	900 ± 100	500 ± 40	2200 ± 100	−0.093	−0.081 ± 0.003

[a] Values are independently determined from CV and used to model SWV.

in the chain were treated individually. As for the simpler model, it was not possible to obtain acceptable fits. However, we cannot exclude the possibility that more complex models which include (in part) a hopping mechanism could also describe the Fcc_3 data. For instance, it is possible that models which combine hopping with nonhopping can fit the data. This could be possible if the electron only hops via one of the heme groups (i.e., heme 4) to the FAD, leaving the other heme groups out of the ET path. Many other complex models may be considered, but all these would have many parameters making a unique analysis or interpretation impossible. Future studies could focus on enzymes with fewer redox-active cofactors to circumvent the need for models in which the redox chain is simplified. However, in each case, care must be taken to ensure that the active site is sufficiently buried into the enzyme to preclude the possibility of a direct, unmediated, electron-tunneling process.

Concluding Remarks

We have shown that square-wave voltammetry provides insight into the intramolecular ET in multicenter enzymes that is complementary to that obtained by other methods. We have studied the ET kinetics to buried FAD groups in two enzymes: fumarate reductases from *S. frigidimarina* (Fcc_3) and *E. coli* (FrdAB). For both proteins, the ET kinetics can be described by Butler−Volmer equations, suggesting that the electrons are transferred directly from the electrode surface to the active site FAD. This might involve a superexchange mechanism via the orbitals of the relaying redox chain. The SWV data of FrdAB could also be described by a mechanism in which electrons are transferred to the FAD via a hopping mechanism involving redox changes at the intermediately located Fe−S clusters that connect the buried FAD to the protein surface.

These results suggest that for Fcc_3 the biological redox chain, which connects the buried FAD group with the protein surface, might function predominantly by increasing the electronic coupling between the donor and acceptor. Fcc_3 contains four hemes (Figure 2) which are all located relatively close to the surface. One of these hemes is also located near the FAD, and a scheme is conceivable in which electrons are transferred to the FAD via only one or two of the hemes. The properties of the Fe−porphyrin, with the strongly delocalized π-orbitals, would be suited to increase the electronic coupling of the FAD to the protein surface that contacts the electrode, enabling electrons to be transferred via a superexchange mechanism. On the other hand, FrdAB contains three Fe−S clusters of which only one is located at the protein surface. This exposed Fe−S cluster does not lie close to the FAD, and only via the other two Fe−S clusters can a pathway to the FAD be envisaged (Figure 2). For FrdAB, the SWV data are not able to distinguish between models based on hopping or nonhopping mechanisms.

Finally, irrespective of the ET model used, the data give a good indication of the maximum ET rate to the active site site FAD group. For Fcc_3, this is equal to k_{max} ($5-6 \times 10^3$ s^{-1}), which is an order of magnitude higher than the catalytic rate ($k_{cat} = 120-250$ s^{-1} [23,24,60]). For FrdAB, the maximum ET rate to the FAD is either $k_{max(FAD)}$ (nonhopping model) or approaches k_1 ($=k_{-2}$) (hopping model). These values correspond well with each other, ranging from 820 to 1500 s^{-1}, which is very close to the fumarate reduction rate $k_{cat} \approx 840$ s^{-1},[61] but much higher than the succinate oxidation rate.[26] Therefore, the rate of fumarate reduction may be limited by intramolecular ET. On

(60) Morris, C. J.; Black, A. C.; Pealing, S. L.; Manson, F. D. C.; Chapman, S. K.; Reid, G. A.; Gibson, D. M.; Ward, F. B. *Biochem. J.* **1994**, *302*, 587−593.

the other hand, the slower succinate oxidation seems not to be limited by ET and can be analyzed by a Michaelis−Menten model that incorporates the potential dimension.[27] As we have shown previously,[62] limiting ET rates can explain the complicated catalytic waves that are observed for fumarate reduction by FrdAB, for example, a boost in the catalytic reduction of fumarate when the potential is lowered below $E^{0'}$ of the [4Fe−4S] cluster.[25,26] The complicated waves support the idea that the electrons are indeed transferred to the FAD via the redox chain.

(61) This value was measured under different conditions (pH 7.0, 25 °C).[26] Note that for a single turnover, two electrons are required. Note also that the value for k_{max} or k_1 is dependent on the assumed cooperativety of ET to the FAD, becoming smaller at higher degrees of cooperativety.

(62) Heering, H. A.; Hirst, J.; Armstrong, F. A. *J. Phys. Chem. B* **1998**, *102*, 6889−6902.
(63) Ethan, M.; Bacon, D. *Methods Enzymol.* **1997**, *277*, 505−524.
(64) Kraulis, P. *J. Appl. Crystallogr.* **1991**, *24*, 946−950.
(65) Connolly, M. L. *Science* **1983**, *221*, 709−713.

In conclusion, these experiments with structurally defined, multicentered redox enzymes represent a new approach to investigate the nature of long-range intramolecular electron transfer. What is now needed are more examples of suitable multicenter enzymes along with site-directed mutants designed to alter systematically the ET energetics.

Acknowledgment. This research was supported by the U.K. EPSRC and BBSRC (Grants 15/C12775, 43/B10492, and 43/B11675) and by the Department of Veterans Affairs and the National Institutes of Health (GM61606). Anne K. Jones thanks the Rhodes Trust and the National Science Foundation for scholarships.

JA012638W